

## Article

# GNSS/AQUA Fusion Study of Atmospheric Response Characteristics and Interaction Mechanisms during the 2022 Tonga Volcanic Eruption

Lulu Ming<sup>1,2,3</sup>, Fuyang Ke<sup>1,4,\*</sup>, Xiangxiang Hu<sup>5</sup>, Wanganyin Cui<sup>2</sup> and Pan Zhao<sup>2</sup>

<sup>1</sup> School of Software, Nanjing University of Information Science & Technology, Nanjing 210044, China; mll9805@163.com

<sup>2</sup> School of Remote Sensing and Geomatics Engineering, Nanjing University of Information Science & Technology, Nanjing 210044, China; 20211235001@nuist.edu.cn (W.C.); zp2359517273@126.com (P.Z.)

<sup>3</sup> College of Geospatial Information, Strategic Support Force Information Engineering University, Zhengzhou 450001, China

<sup>4</sup> Wuxi Research Institute, Nanjing Information Engineering University, Wuxi 214100, China

<sup>5</sup> School of Resources and Environmental Engineering, Tianshui Normal University, Tianshui 741001, China; huxiang0915@163.com

\* Correspondence: kefuyang@nuist.edu.cn

**Abstract:** A large-scale underwater volcanic eruption occurred at the volcano of Hunga Tonga-Hunga Ha'apai (HTHH) on 15 January 2022. At present, there is no consensus on the ionospheric response characteristics and interaction mechanism during volcanic eruptions. Based on the Global Navigation Satellite System (GNSS), AQUA satellite's Atmospheric Infrared Sounder (AIRS), the experiment studies the response characteristics of the ionosphere and gravity waves during the eruption of the volcano and their interaction mechanisms and the International Real-Time Geomagnetic Observation Network (INTERMAGNET). First, a geomagnetic anomaly was detected before the eruption, which caused variations in the ionospheric *VTEC* (Vertical Total Electron Content) by about 15 TECU. Based on the IGS (International GNSS Service) observations, the *VTEC* distribution between 60° north and south latitudes was retrieved. The results show that before and after the eruption of Tonga Volcano, significant ionospheric anomalies were observed to the south, northwest and southwest of the volcano, with a maximum anomaly of 15 TECU. The study indicates that the geomagnetic anomaly disturbance is one of the precursors of volcanic eruption and has a certain degree of impact on the ionosphere. A correlation between geomagnetic anomalies and ionospheric anomalies was found to exist. The vast impact from the volcanic eruption excites gravity waves over the surface, which then propagate longitudinally, further perturbing the ionosphere. It is also detected that the ionospheric anomaly perturbation has a high coincidence effect with the gravity wave anomaly. Therefore, the gravity waves generated by atmospheric variations are used to explain the ionospheric perturbation phenomenon caused by volcanic eruptions.

**Keywords:** continuous geomagnetic signal; gravity waves; abnormal *VTEC*; interaction mechanism



**Citation:** Ming, L.; Ke, F.; Hu, X.; Cui, W.; Zhao, P. GNSS/AQUA Fusion Study of Atmospheric Response Characteristics and Interaction Mechanisms during the 2022 Tonga Volcanic Eruption. *Atmosphere* **2023**, *14*, 1619. <https://doi.org/10.3390/atmos14111619>

Academic Editors: Nigang Liu and Si Liu

Received: 25 September 2023

Revised: 25 October 2023

Accepted: 26 October 2023

Published: 28 October 2023



**Copyright:** © 2023 by the authors. Licensee MDPI, Basel, Switzerland. This article is an open access article distributed under the terms and conditions of the Creative Commons Attribution (CC BY) license (<https://creativecommons.org/licenses/by/4.0/>).

## 1. Introduction

On 15 January 2022, a violent volcanic eruption occurred at the Hunga Tonga—Hunga Ha'apai (HTHH) submarine volcano (174°24'21.6" W, 20°32'34.8" S). The violent eruption of this volcano was the largest so far in the 21st century. The eruption produced large quantities of ash, gas and water vapor [1,2]. It has attracted the attention of experts in many fields, including meteorology, seismology, volcanology, high-performance and visualization computing, from all over the world. The monitoring of submarine volcanic activity and the study of atmospheric response during eruptions are not only conducive to the understanding of the mechanisms of crustal movement and inter-atmospheric interaction but also of great significance for the prevention and control of volcanic disaster risks.

Volcanic eruptions are a natural phenomenon, usually accompanied by earthquakes. It affects both the ionosphere and the upper atmosphere. In recent years, with the continuous development of GNSS technology, the means of observing the ionosphere using GNSS and the observation accuracy have been continuously improved. At present, increasing numbers of scholars are utilizing TEC to detect ionospheric variations [3–5]. Zakharenkova, I.E et al. [6] obtained Total Electron Content (TEC) data using GPS (Global Positioning System) observations, which provided information on the ionosphere in the study area and visualized anomalous ionospheric features. Numerous studies have found that anomalous ionospheric variations do exist before and after earthquakes. After the HTHH eruption on the 15th, atmospheric gravity waves that appeared to be associated with the eruption were detected at numerous observatories around the world [7]. These waves are likely to propagate upwards into the upper atmosphere, generating electron density perturbations in the ionosphere. In fact, TIDs were detected by total electron content (TEC) analysis, which may be caused by atmospheric waves [8].

In addition, for volcanoes characterized by submarine eruptions, conventional seismological or geodetic monitoring is usually insufficient because the energy of the impending eruption is not large enough to accumulate even in the absence of magmatic movement [9]. Continuous observations of the total geomagnetic intensity are often used to evaluate volcanic activity because they can reveal the accumulation of energy within an active volcano. Several attempts have been made to monitor the geostress state or temperature inside volcanoes by observing the surface geomagnetic field, and volcanic magnetic changes associated with anomalous volcanic activity have been reported for many volcanoes [10,11]. Adushkin, VV et al. detected changes in geomagnetism during the HTHH eruption using the INTERMAGNET network observatory. The results indicate that the eruption was accompanied by atmospheric wave disturbances and strong magnetic and electric field changes at the distance from the epicenter [12].

In summary, many scholars have studied the mechanism of TIDs and gravity waves triggered by the eruption of the volcano, and many results have been achieved. However, there is a lack of a comprehensive analysis of the characteristics and interaction mechanisms of the global ionospheric and geomagnetic activity and the response of the atmosphere above before and after the eruption of the volcano. In this paper, Vertical Total Electron content (VTEC) from the GNSS measurement is utilized to investigate ionospheric variations caused by volcanic eruption. The spatial and temporal characteristics of the ionosphere are analyzed in the prophase, metaphase, and anaphase of volcanic eruptions. The possible coupling mechanism of volcano-induced ionospheric variations and atmospheric fluctuations are discussed by combining the total intensity of the geomagnetic signal and gravity wave information.

## 2. The Variations of VTEC Calculation Method

The total electron content (TEC) is defined as the line integral of the electron density on a given ray path. This tilted TEC (*STEC*) corresponds to the total number of free electrons along a cylindrical path with a cross-sectional area of 1 m<sup>2</sup>. When the TEC is calculated over a vertical path in the local zenith direction, it is called the vertical total electron content (*VTEC*) [13]. Arikan, Erol, and Arikan [14] devised a technique to estimate the *VTEC* by combining the received signals from all satellites that are 10° above the GNSS elevation limit. The algorithm can be successfully applied to the ionosphere in high, mid-latitude, and equatorial regions on calm and disturbed days.

In this paper, IONOLOAB is used to calculate *VTEC* [15] Product data from satellite bias and receiver bias are used to eliminate bias. The following equation calculates *STEC*.

$$STEC_m(n) = \frac{P2_m(n) - P1_m(n)}{A} \frac{f_1^2 f_2^2}{f_1^2 - f_2^2} + s_m + r \quad (1)$$

where the receiver of the GNSS station records the signals transmitted at two L-band frequencies,  $f_1 = 1575.42$  MHz,  $f_2 = 1227.60$  MHz. The time delays that occur as these signals propagate through the ionosphere are converted to the Pseudo-range and recorded as  $P1$  and  $P2$  signals.  $A = 40.3 \text{ m}^3/\text{s}^2$ ;  $m$  is the number of satellites;  $n$  is the number of samples;  $S_m$  is the bias for the  $m$ -th satellite,  $r$  is the receiver bias.

The  $VTEC$  can be obtained by projecting the calculated  $STEC$  to the local zenith direction using the over-mapping function  $M(\epsilon)$  [13,16]. The following equation calculates the  $VTEC$ :

$$VTEC_m(n) = STEC_m(n) / M(\epsilon_m(n)) \tag{2}$$

$$M(\epsilon_m(n)) = \left[ 1 - \left( \frac{R \cos \epsilon_m(n)}{R + h} \right)^2 \right]^{-\frac{1}{2}} \tag{3}$$

In the above equation,  $\epsilon_m(n)$  is the elevation angle in the receiver coordinates of the  $m$ th satellite of the  $n$ th sample,  $R$  is the radius of the Earth, and  $h$  is the height of the ionospheric penetration point.

We take a time window of about two weeks before the eruption (i.e., 1 January 2022–13 January 2022), and compute the average  $VTEC$  value  $\bar{X}_t$  and the instantaneous standard deviation  $\Delta_t$  corresponding to each calendar element during this time window, which is given in the following equations:

$$\bar{X}_t = \frac{(X_t)_1 + (X_t)_2 + \dots + (X_t)_{13}}{13} \tag{4}$$

$$\Delta_t = \sqrt{\left[ (X_t)_1 - \bar{X}_t \right]^2 + \left[ (X_t)_2 - \bar{X}_t \right]^2 + \dots + \left[ (X_t)_{13} - \bar{X}_t \right]^2} \tag{5}$$

where  $t$  is the time of the calendar element;  $(X_t)_1, (X_t)_2, \dots, (X_t)_{13}$  are the  $VTEC$  values of the corresponding days in the time window corresponding to the time of the calendar element. On this basis, the ionospheric anomaly is determined by twice the standard deviation above and below the mean value, and the following formula calculates the limit expected value:

$$\begin{cases} (VTEC_{up})_t = \bar{X}_t + 2 * \Delta_t \\ (VTEC_{down})_t = \bar{X}_t - 2 * \Delta_t \end{cases} \tag{6}$$

where  $(VTEC_{up})_t$  and  $(VTEC_{down})_t$  are the upper and lower bounds, respectively. To determine  $VTEC$  variations caused by volcanic eruptions, data sets 14, 15, and 16 were used as test set data.  $VTEC_t$  indicates the  $VTEC$  value of the epoch on the day when the abnormal value is detected. The outlier of  $\Delta VTEC_t$  is calculated with the following formula:

$$\Delta VTEC_t = \begin{cases} VTEC_t - (VTEC_{up})_t [VTEC_t > (VTEC_{up})_t] \\ VTEC_t - (VTEC_{down})_t [VTEC_t < (VTEC_{down})_t] \\ 0 [(VTEC_{down})_t < VTEC_t < (VTEC_{up})_t] \end{cases} \tag{7}$$

### 3. Datasets

#### 3.1. Solar and Geomagnetic Activity

Ionospheric variations are generally influenced by solar activity and geomagnetic disturbance. In order to accurately analyze the response of the ionosphere to volcanic eruptions, The solar F10.7 radio flux index (F10.7), Disturbance Strom Time Index (Dst), and AP are used to determine the solar and geomagnetic activities, respectively. These indexes are collected  $\pm 15$  days centered on volcanic eruptions and their variations are shown in Figure 1. The solar activity is usually determined using the solar F10.7 radio flux index (F10.7). The variations in the F10.7 index can classify the solar activity into low level ( $70 \text{ sfu} < F10.7 < 100 \text{ sfu}$ ), medium level ( $100 \text{ sfu} < F10.7 < 150 \text{ sfu}$ ), and high level ( $150 \text{ sfu} < F10.7$

< 250 sfu). The geomagnetic activity was judged using the Dst and Ap indices. Among them, magnetic storms can be classified as strong ( $Dst < -100$  nT), medium ( $-100$  nT <  $Dst < -50$  nT), and weak ( $-50$  nT <  $Dst < -30$  nT) according to the variations of the Dst index (Ke et al., 2018). In Figure 1a, the Dst decreases quickly to about  $-90$  nT and recovers to  $-30$  nT around 15 January 2022, indicating that a moderate magnetic storm occurred. The Ap variations in Figure 1b confirm that. As illustrated in Figure 1c, the magnitudes of F10.7 range from 85 to 130 sfu, which suggests that the solar activity has been low to moderate during the eruption. Therefore, the effects of magnetic storms on the ionosphere cannot be ignored when studying the effects of volcanic eruptions on ionospheric variations [17].

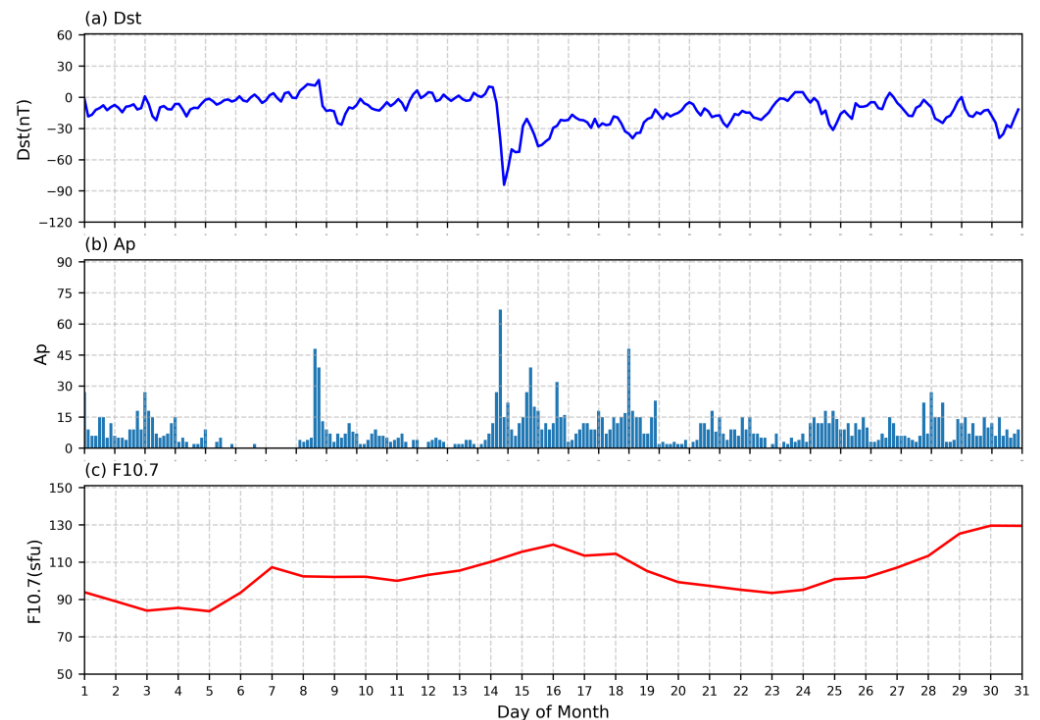


**Figure 1.** The solar index F10.7, the Dst and Ap indexes of the geomagnetic activity from 1 to 31 January 2022.

### 3.2. Data

A violent eruption occurred on 15 January 2022, at the submarine volcano of Hunga Tonga-Hunga Ha’apai (HTHH), Tonga, a South Pacific island nation. The total geomagnetic intensity data are obtained from the International Real-Time Geomagnetic Observatory Network (INTERMAGNET). The only operating observatories close to HTHH and its magnetic conjugate point were API (Apia—Western Samoa, geographic coordinates  $13.82^{\circ}$  S,  $171.78^{\circ}$  W). The data sampling interval is 30 s. The distribution of IGS stations is shown in Figure 2. The data of IGS stations between  $60^{\circ}$  north and south latitude from 1 January 2022 to 31 March 2022, were selected to calculate the ionospheric changes before and after the volcanic eruption. In addition, the experiment uses the  $4.3 \mu\text{m}$  dataset and the  $15 \mu\text{m}$  “high” dataset that Hoffmann et al. [18,19] provided for gravity wave detection. The Atmospheric Infrared Surveyor (AIRS) dataset was obtained on board the NASA AQUA satellite. The detection method is based on the  $4.3 \mu\text{m}$  and  $15 \mu\text{m}$  brightness temperatures in the  $\text{CO}_2$  baseband measured in AIRS. Considering the 109 orbital trajectories of the satellite, the peak events are detected based on the brightness temperature variations using a radiative transfer model and an optimal estimation retrieval scheme. Thus the gravity wave distribution is obtained.

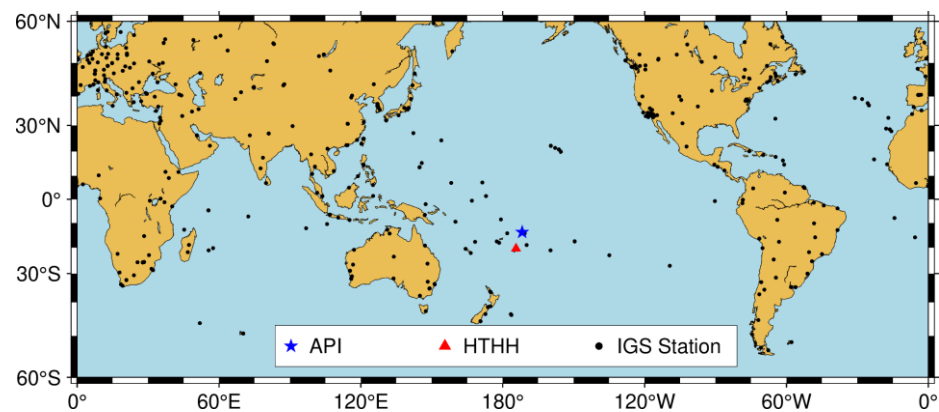


Figure 2. Global Positioning System (GPS) stations of IGS and Location of HTHH and API.

### 4. Results

#### 4.1. Continuous Geomagnetic Signal

The continuous geomagnetic signal can analyze the volcano state, and to study the interaction mechanism between gravity waves, geomagnetism, and ionospheric variations, the total intensity of the geomagnetic signal from 1 to 31 January 2022, was first selected using the API of the geomagnetic observatory near the volcano. Figure 3 shows the variations in the total geomagnetic signal intensity in the month of the volcanic eruption. It can be seen in the selected 30 days that the total geomagnetic intensity shows periodic and regular variations before the occurrence of the volcanic eruption event. It varies between 38,750 nT and 38,850 nT within 24 h. After the volcanic eruption, the position of the red circle in Figure 4 shows an overall decreasing trend of the total geomagnetic signal intensity due to the volcano’s influence. The total geomagnetic intensity hovered around 38,850 nT during 15–16 days and reached the lowest value in the interval. To further remove the cyclical effect of the total geomagnetic intensity, 13 days are used as the background window to remove the effect of the background total geomagnetic intensity using the standard deviation. The results are shown in Figure 4. It could be seen that the geomagnetic anomaly was about  $-50$  nT on the night of 14 January 2022, during the pre-eruption period, followed by a moderately active state of geomagnetic activity on the day of the eruption. This state persisted until 16 January 2022.

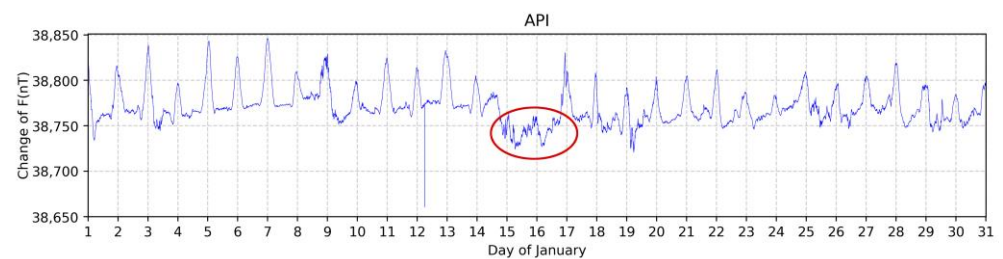


Figure 3. The Variations of Geomagnetic Signal.

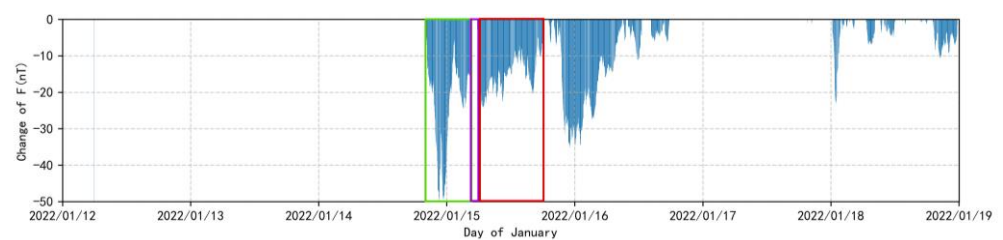
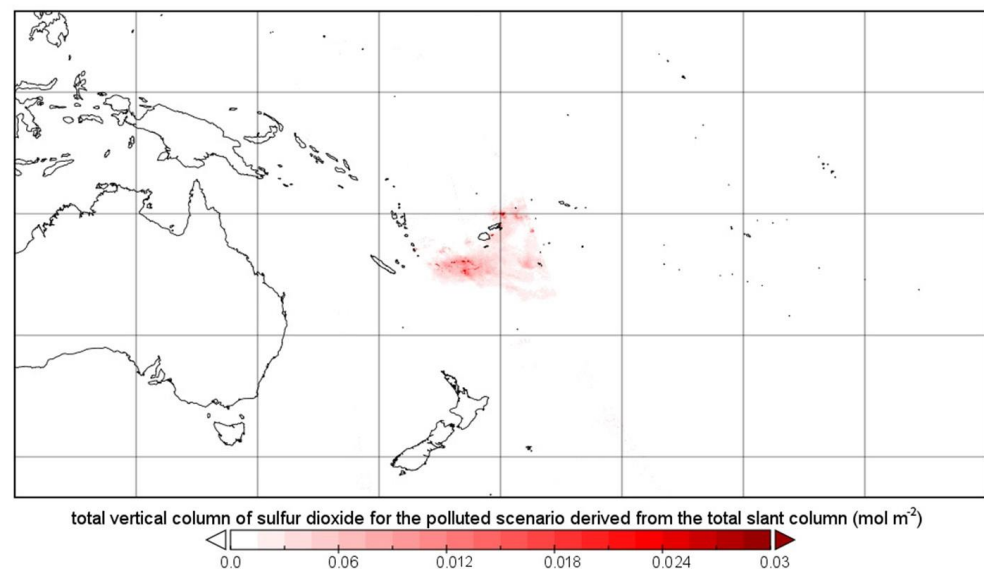


Figure 4. Geomagnetic Variations anomalies with the total background geomagnetic intensity removed.

The changes in the magnetic signal of the volcano are mainly caused by the magma movement and the temperature changes on the volcano's surface. Considering the complexity of the magma movement and the chemical and thermal processes occurring inside, the  $\text{SO}_2$  produced by the volcanic eruption was further probed in Figure 5. It is found that volcanic eruptions bring about a significant effect on temperature changes. Related studies have shown that gravity waves often accompany temperature changes [20]. Therefore, the effect of volcanic eruptions on gravity wave generation was further explored.



**Figure 5.** The Variations of  $\text{SO}_2$  on 15 January 2022.

#### 4.2. Gravity Wave Response to HTHH

To further analyze the post-eruption interaction mechanism of the volcano. Strong atmospheric gravity waves were observed in the stratosphere 8.5 h after the eruption using the Atmospheric Infrared Surveyor (AIRS), a satellite instrument near Tonga [21]. The atmospheric gravity wave properties were determined from horizontal fluxes for the  $4.3 \mu\text{m}$  data set and the  $15 \mu\text{m}$  “high” data set. As the results in Figure 6 show, since the density decreases with height, the wave amplitude is bound to increase with height according to the continuum of energy flow. Therefore, when the monitoring height reaches 40–45 km, it is evident that the amplitude becomes more extensive, and the fluctuations are more pronounced. Thus, atmospheric gravity waves excited by volcanic eruptions have a large amplitude and a broad spatial and temporal range of spectra in the mesosphere. During the geomagnetic disturbance, the vertical propagation velocity of gravity waves and the magnitude of their vertical wavelengths are similar to the exponential variations of geomagnetic disturbance AE with a linear relationship. The vertical altitude variations can reach 520 km [22], which can cause variations in the ionosphere at altitudes of 80–600 km.

It is further confirmed that the volcanic eruption caused the atmospheric gravity wave disturbance and the analyzed gravity wave anomaly changes before and after the explosion. As shown in Figure 7b, the volcanic eruption caused a circular disruption in the area above it at the beginning of 40–45 km on 15 January 2022. Figure 7a,c show no significant gravity waves appear above the volcano on the 14th and 15th. This is due to the rapid rise of hot air and ash from the volcanic eruption, which causes the air molecules in the atmosphere to oscillate in the air column by vertical perturbations. The atmospheric gravity waves then propagate outward in a circular pattern in the vertical direction. The average speed of its propagation is 310 m/s, which is the same as the atmospheric gravity wave propagation speed. The gravity wave transports energy with kinetic energy from the lower atmosphere to the upper atmosphere. And have the necessary characteristic amplitude and phase velocity to penetrate the ionosphere and excite responsive ionospheric variations [23].

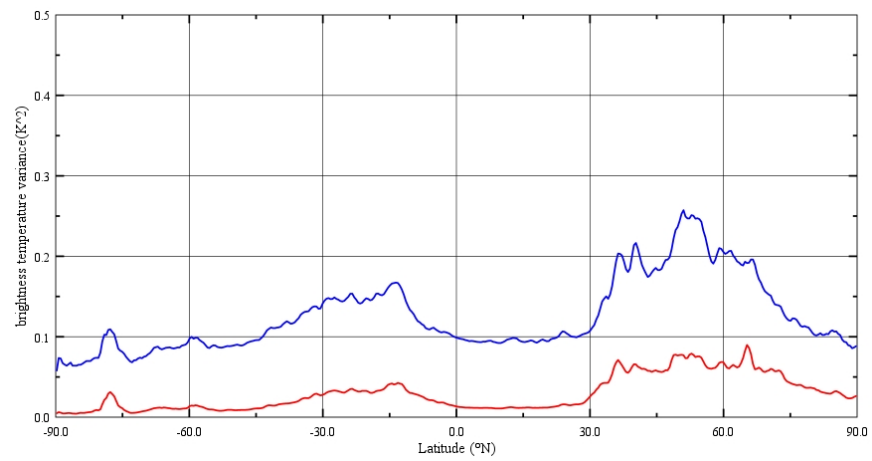


**Figure 6.** Brightness Temperature Variance at 4.3 Micron (Blue Line) and 15 Micron (High Altitudes) (Red Line) on 15 January 2022.

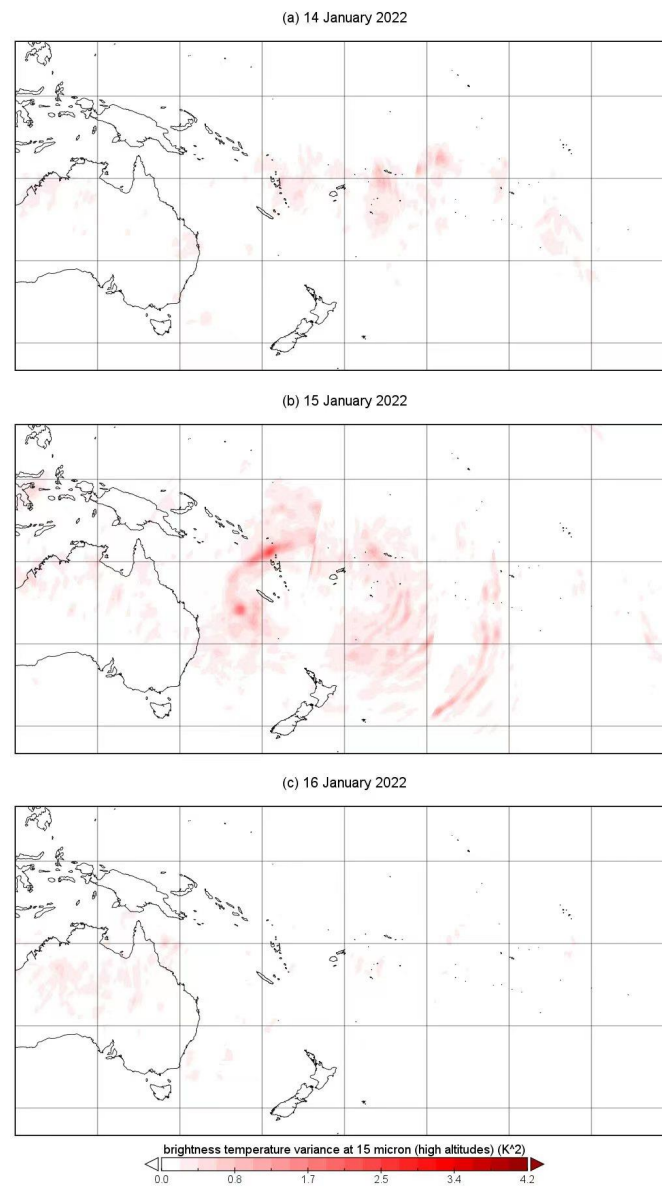


**Figure 7.** Brightness Temperature Variance at 15 Micron (High Altitudes) on 14 January 2022 (a), 15 January 2022 (b) and 16 January 2022 (c).

#### 4.3. GNSS VTEC Response to HTHH

To investigate the interaction mechanism of volcanic eruption generation. In this paper, the experiment first excludes the perturbation of ionospheric anomalies by magnetic storms and compares the GNSS VTEC of IGS stations under equivalent magnetic storms and standard conditions (equivalent magnetic storms occurred on 4 November 2021, and 15 January 2022, and normal conditions on 20 December 2021). As shown in Figure 8, three stations (FRDN/GOL2/THTI) are selected for equal distribution, where the ionospheric variations on the day of the volcanic eruption are significantly more abnormal than the other two days. The ionospheric anomaly caused by the magnetic storm on 4 November 2021, is significantly smaller than that caused by the volcanic eruption. Based on this, the response of GNSS VTEC to the volcanic eruption from 1 to 16 January 2022 is analyzed by excluding the perturbation of ionospheric anomalies by magnetic storms. To determine that the volcanic eruption causes the VTEC perturbation, the 14th, 15th, and 16th data sets are used as the test set data. The mean value of the VTEC and the corresponding momentary standard deviation are calculated for the period from January 1 to 13, two weeks before the volcanic eruption. The mean value plus or minus twice the standard deviation is the VTEC average interval. The background ionospheric data were thus removed from the test set data. The VTEC anomalies were compared between the 14th, 15th, and 16th latitudes.

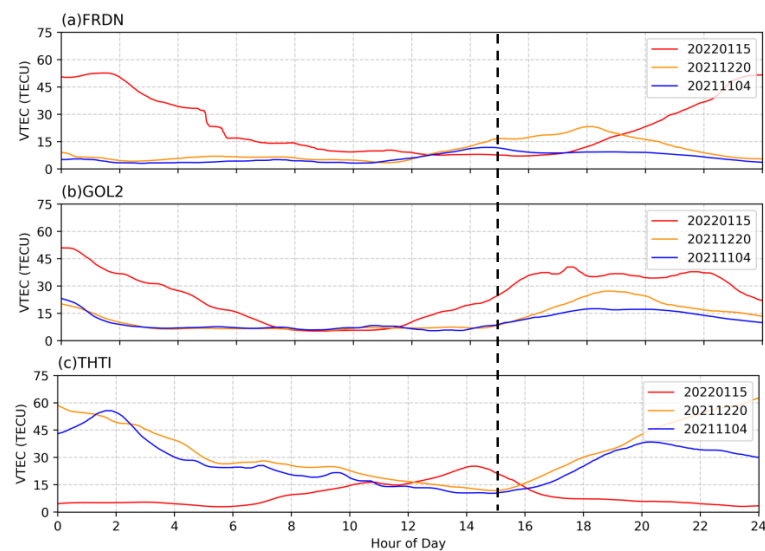


**Figure 8.** The VTEC in Three Different Cases.

As shown in Figure 9, the background values of ionospheric variations were removed the day before the eruption (14 January 2022). It can be found that small changes in VTEC were detected in the northwest of the volcano starting at UTC 20:00 (Figure 9k). The variations were detected increasing to about 10 TECU at UTC 22:00 (Figure 9l). At the same time, about  $-5$  TECU was detected southeast and southwest of the volcano. The overall changes are basically consistent with the changes in ionospheric anomalous perturbations in GIM.

On the day of the eruption on 15 January 2022, the anomalous ionospheric variations with background values removed broke the regularity and periodicity of the ionospheric distribution. At UTC 00:00 (Figure 10a), VTEC variations were detected in the south, northwest, and southwest of the volcano, ranging from about  $-5$  to 10 TECU. At the same time, the variation was detected in the southwest of the volcano at about  $-10$  TECU, but a comparison of the anomaly distribution of the GIM ionosphere revealed that the anomaly did not exist. Combined with the site distribution, it is found that the anomaly distribution interpolated on this basis has errors due to the scarcity of GNSS sites in the southwest of the volcano. Subsequently, after the eruption of the volcano (UTC 04:00, Figure 10a), an anomalous perturbation of about  $-10$  TECU was observed near the equator,

and a perturbation of about 5 to 15 TECU was also observed in the northern part of the volcano. Until UTC 20:00 (Figure 10k), the anomalies gradually decreased in each region and resumed the obvious trend. Except for the missing site region, the overall trend of the other regions is very similar to that of GIM.

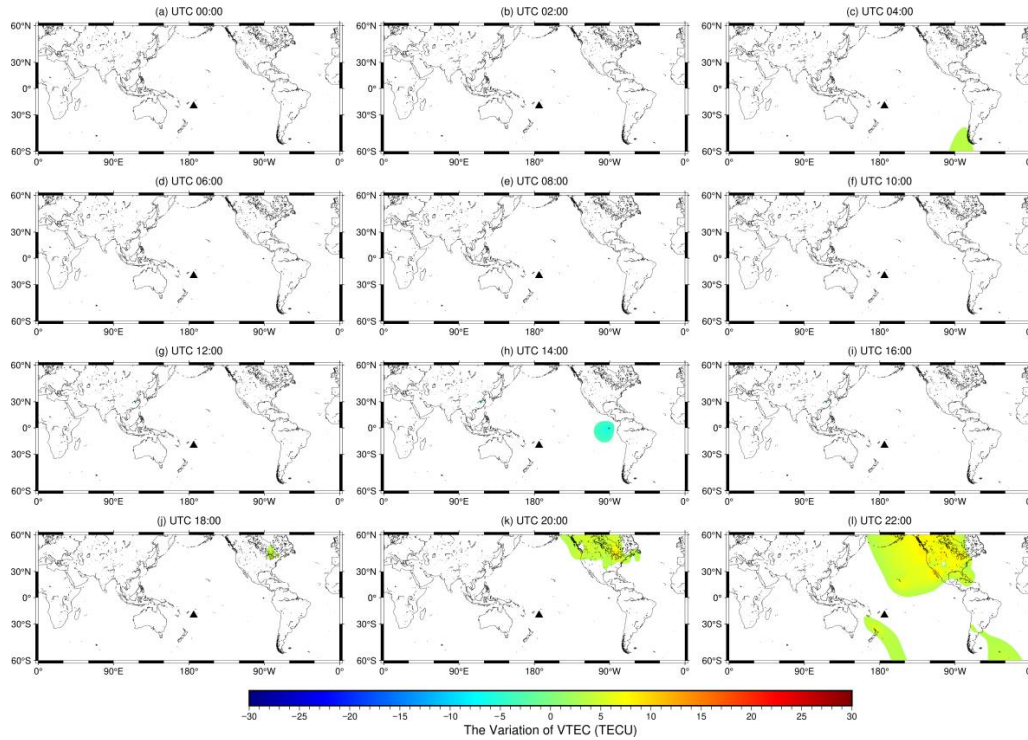


**Figure 9.** The Abnormal VTEC between 60 Degrees North and 60 Degrees South on 14 January 2022 and the black triangle represents the location of the volcano.

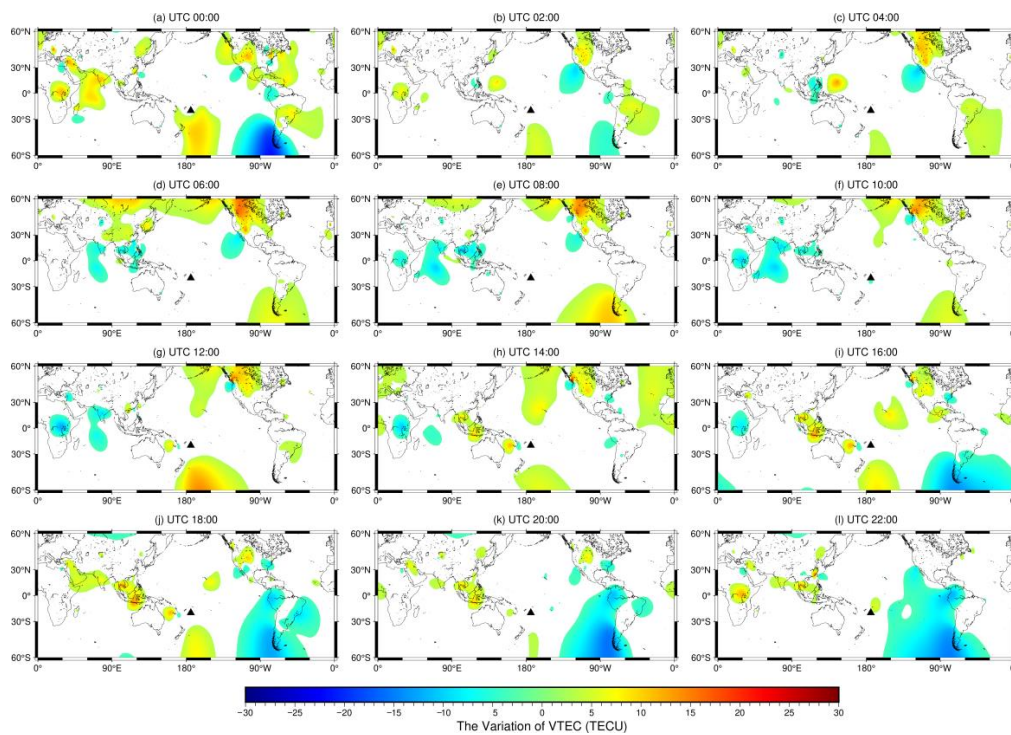


**Figure 10.** The Abnormal VTEC between 60 Degrees North and 60 Degrees South on 15 January 2022 and the black triangle represents the location of the volcano.

As shown in Figure 11 one day after the 16 January 2022 eruption, UTC 00:00–08:00 (Figure 11a–e), the eruption-induced ionospheric disturbances are still present. However, most of the area has returned to normal, and only a small-scale disturbance of about  $-5$  to  $5$  TECU exists at  $60^\circ$  N north of the volcano.

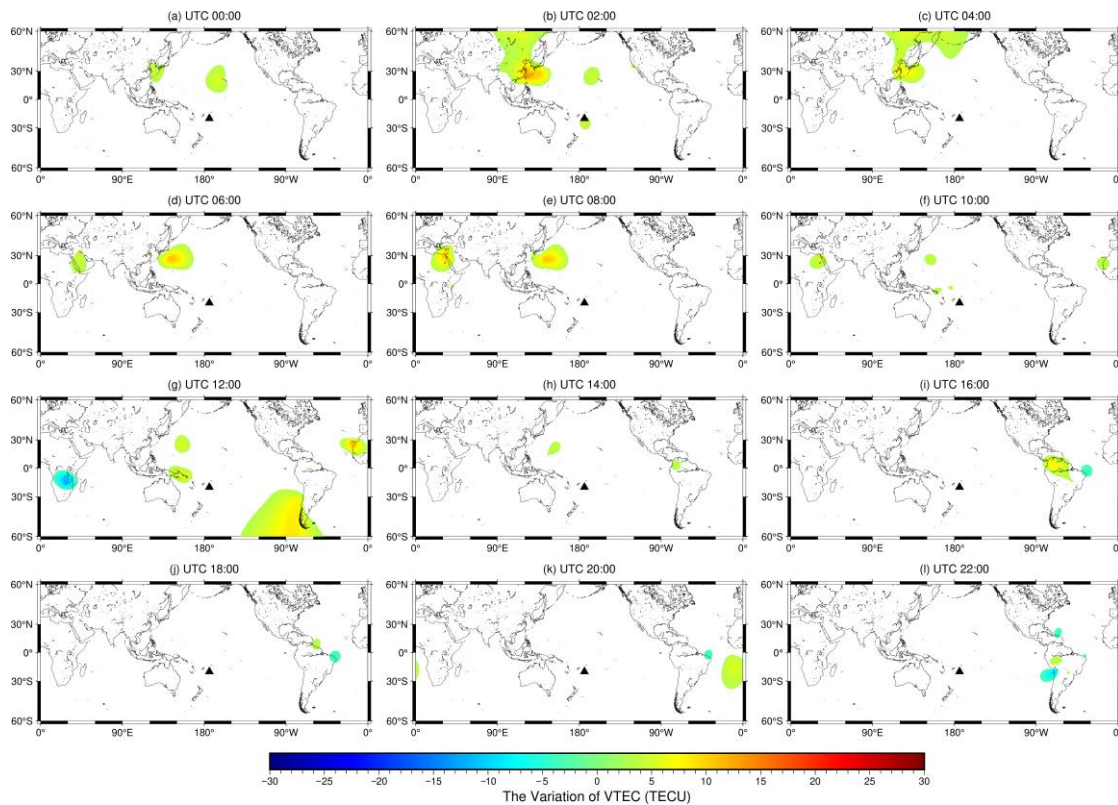


**Figure 11.** The Abnormal VTEC between 60 Degrees North and 60 Degrees South on 16 January 2022 and the black triangle represents the location of the volcano.

## 5. Discussion

The Volcano is located on the southwest Pacific plate boundary. It results from the subduction of the Indo-Australian plate into the Pacific plate [24], which causes mantle magma to rise into the Earth's crust [25]. And erupts in the plate boundary region, forming volcanoes. The violent eruption of the volcano on 14–15 January 2022, was the largest of the 21st century so far. The explosion led to the formation of airwaves and electrical and magnetic effects [12]. Significant anomalies in the geomagnetic signal, ionosphere, and gravity waves were excited in the upper atmosphere.

Anomalous responses caused by irregular events (e.g., geomagnetic storms and solar flares) may produce large- and mesoscale TIDs moving from high latitudes to the equator. Figure 3 shows the 15-day record of geomagnetic and solar activity indices before and after the eruption. The Dst and Ap indices were high from 18:00 UTC on 14 January 2022, to 02:00 UTC on 15 January. During that time, we experienced a moderately strong geomagnetic storm, which led to anomalously sharp fluctuations in the geomagnetic signal, revealing to some extent the cause of the mesoscale nonvolcanic disturbances in the ionosphere during this time [26]. The green box verifies this conclusion in Figure 4 and the content of Figure 10a,b. We were followed by a gradual recovery of the magnetic storm [26]. At the same time, the gathering and uplift of magma prior to eruption may have led to the demagnetization of the crust by increasing the temperature above the Curie temperature [27]. The content of the purple box in Figure 4 verifies the recovery of the magnetic storm after a moderately intense geomagnetic storm and the return of the geomagnetic signal to normal.

Figure 3 Solar activity on day 15 was also moderate ( $F_{10.7} = 116$ ), suggesting that another significant factor on the day of the event led to TIDs. The volcano's massive eruption at 04:00 UTC on 15 January 2022, produced a plume of up to 58 km high, with the ash continuing throughout the night, and the eruption lasted 12 h [28]. This was the first time the volcano had been in a state of volcanic eruption, and it was not the only time the eruption occurred in the Earth's magnetic field. However, it was also the only time the volcano was in a state of volcanic eruption. As magma begins to accumulate and sublimate toward the surface, its movement causes rupture and deformation of subsurface rocks, which leads to changes in the geomagnetic field. Telesca L et al. [29] found that changes in the magnetic signature of volcanoes arise primarily from changes in volcanic temperature caused by magmatic movement. The magnetic variations are generated by stress redistribution caused by magma intrusion at different depths [10]. Its magnetic changes occur almost simultaneously with the rise of the magma pulse, leading to significant temperature changes above the volcano [29]. The red box in Figure 4 reflects the anomalies in the geomagnetic signal due to the eruption.

In addition, eruptions produce a large number of gases [1,5], including  $\text{SO}_2$ ,  $\text{CO}$ , water vapor ( $\text{H}_2\text{O}$ ),  $\text{CO}_2$ ,  $\text{H}_2\text{S}$ ,  $\text{HCl}$ , hydrogen fluoride, hydrogen bromide,  $\text{CH}_4$ ,  $\text{CH}_3\text{Cl}$ ,  $\text{H}_2$ , and heavy metals [30]. The process of accumulating gases in the atmosphere can bring about the ionization of air, a critical key driver of possible electrical phenomena in the atmosphere and ionosphere, altering the Earth's global circuitry [31,32]. Figures 9–11 trace the state of TIDs before and after volcanic eruptions using IGS observatories around the globe. Figures 10k,l and 11a,b validate the anomalous ionospheric fluctuations due to a moderate-intensity geomagnetic storm. Figure 11c–l verifies TIDs caused by volcanic eruptions. The results show that the ionospheric electron density is greatly perturbed around the eruption site and in the region extending northward. The most robust ionospheric response associated with the 15 January 2022 eruption is produced far from the epicenter. This is the same as Themens et al. [1] observed.

At the same time, it has been shown that the ground motion of gravity waves is excited by the interaction between the solid Earth and the ionosphere [33]. Gravity waves transport energy and kinetic energy from the lower to the upper atmosphere. Gravity waves have the necessary characteristic amplitudes and phase velocities to penetrate the ionosphere and excite responsive ionospheric disturbances [23]. This is because gravity waves exist over an extensive altitude range (50–500 km) from the mesosphere to the ionosphere. At such altitudes, due to the presence of charged and neutral particles, the vortex structures generated by gravity waves carry captured particles, resulting in the transport of plasma particles through the atmosphere [34]. The volcano's eruption on January 15 induced a strong air mass movement, which resulted in significant changes in the atmospheric pressure at significant distances. Liu X et al. [35]. detected the presence of solid gravity waves with amplitudes more significant than 30 K, twice the regular gravity waves, on the 15th. As shown in Figure 7, the gravity wave fluctuations occurring above the volcano on the 14th–16th days were analyzed in comparison. Compared to the 14th and 16th days, an apparent ring-shaped fluctuation appeared over the volcano on the 15th day, and the frequency of its fluctuation was significantly higher than that on the other two days. It is further verified that the volcano's eruption caused the atmospheric gravity wave disturbance.

In this study, we systematically analyzed the response characteristics and interaction mechanisms among geomagnetic signals, ionosphere, and atmospheric disturbances by using the International Real-Time Geomagnetic Observation Network (INTERMAGNET), the IGS monitoring station and the Atmospheric Infrared Sounder (AIRS).

## 6. Conclusions

In this paper, the gravity waves and ionospheric variations generated during the eruption of the volcano on 15 January 2022, are presented, and the ionospheric and gravity

wave response characteristics and their interaction mechanisms are analyzed. The main findings are summarized as follows:

1. The API of geomagnetic sites near the volcano was detected and found that the volcanic eruption caused a decrease in the total geomagnetic intensity in the vicinity, leading to some extent to ionospheric anomalies.
2. The gravity waves presented in this study were obtained based on AIRS on the AQUA satellite with longitudinal propagation characteristics, and ionospheric anomalies were also detected in the region, showing the same trend.
3. Ionospheric anomalies were observed before and after the eruption using GNSS data, with significant anomalies mainly to the south, northwest and southwest of the volcano, with a maximum anomaly of 15 TECU. On the second day of the eruption, VTEC anomalies were observed on the volcano's north and east sides, disrupting the ionospheric distribution's regularity and periodicity
4. Before the eruption, total geomagnetic intensity anomalies were detected using the geomagnetic site (API) on 14 January 2022, in Figure 4. The geomagnetic solid anomaly resulted in an anomalous ionospheric variation of about 10 TECU at UTC 22:00 on 14 January 2022, in the western part of the volcano in Figure 9. The phenomenon persisted until UTC 00:00 on the 15th; thereafter, strong gravity waves were induced and detected on the volcano with the considerable impact triggered by the eruption in Figure 7b. In Figure 10, gravity waves propagate vertically upward into the ionosphere, producing variations of about 5 to 15 TECU in the southern, northeastern, and northwestern parts of the volcano. Based on GNSS data, INTERMAGNET data and 15  $\mu\text{m}$  datasets provide essential information about geomagnetic, gravity wave and ionospheric variations. In this way, the ionospheric and gravity wave response characteristics and their interaction mechanisms during volcanic eruptions are presented.

**Author Contributions:** Conceptualization, L.M. and F.K.; methodology, L.M. and F.K.; validation, L.M., X.H. and P.Z.; formal analysis, L.M. and X.H.; investigation, L.M., X.H. and P.Z.; resources, L.M. and P.Z.; data curation, L.M.; writing—original draft preparation, L.M.; writing—review and editing, L.M., F.K. and W.C.; visualization, L.M. and W.C.; supervision, L.M.; project administration, F.K.; funding acquisition, F.K. All authors have read and agreed to the published version of the manuscript.

**Funding:** This research was funded by Natural Science Foundation of Jiangsu Province, grant number BK20211037, the sixth “333 Talents” training and funding project in 2022, grant number BRA2022042, and Jiangsu Province key research and development plan, grant number BE2021622.

**Institutional Review Board Statement:** Not applicable.

**Informed Consent Statement:** Not applicable.

**Data Availability Statement:** The total geomagnetic intensity data are obtained from the International Real-Time Geomagnetic Observatory Network (INTERMAGNET), which are publicly available at <https://intermagnet.github.io/> (accessed on 1 January 2020 to on 31 January 2020). Ionospheric data can be accessed at <https://cdis.nasa.gov/archive/gnss/data/daily/> (accessed on 1 January 2020 to on 16 January 2020). Gravity wave data are available at [https://datapub.fz-juelich.de/slcs/airs/gravity\\_waves/data/projects/tonga](https://datapub.fz-juelich.de/slcs/airs/gravity_waves/data/projects/tonga) (accessed on 14 January 2020 to on 16 January 2020).

**Acknowledgments:** We acknowledge the International Real-Time Geomagnetic Observatory Network for the total geomagnetic intensity data and International Association of Geodesy (IAG) for providing us with IGS raw data.

**Conflicts of Interest:** The authors declare no conflict of interest.

## References

1. Themens, D.R.; Watson, C.; Žagar, N.; Vasylykevych, S.; Elvidge, S.; McCaffrey, A.; Prikryl, P.; Reid, B.; Wood, A.; Jayachandran, P. Global propagation of ionospheric disturbances associated with the 2022 tonga volcanic eruption. *Geophys. Res. Lett.* **2022**, *49*, e2022GL098158. [[CrossRef](#)]
2. Zhang, S.-R.; Vierinen, J.; Aa, E.; Goncharenko, L.P.; Erickson, P.J.; Rideout, W.; Coster, A.J.; Spicher, A. 2022 tonga volcanic eruption induced global propagation of ionospheric disturbances via lamb waves. *Front. Astron. Space Sci.* **2022**, *9*, 871275.
3. Ke, F.; Wang, J.; Tu, M.; Wang, X.; Wang, X.; Zhao, X.; Deng, J. Morphological characteristics and coupling mechanism of the ionospheric disturbance caused by super typhoon sarika in 2016. *Adv. Space Res.* **2018**, *62*, 1137–1145.
4. Tang, L.; Li, Z.; Zhou, B. Large-area tsunami signatures in ionosphere observed by gps tec after the 2011 Tohoku earthquake. *GPS Solut.* **2018**, *22*, 93. [[CrossRef](#)]
5. Zhang, Y.; Zhong, H.; Zhang, T.; Huang, R.; Feng, J. Analysis of low latitude ionospheric changes before the May 26, 2019 earthquake in northern peru. *J. Geod. Geodyn.* **2023**, *43*, 135–140.
6. Zakharenkova, I.E.; Shagimuratov, I.I.; Tepenitzina, N.Y.; Krankowski, A. Anomalous modification of the ionospheric total electron content prior to the 26 september 2005 peru earthquake. *J. Atmos. Sol.-Terr. Phys.* **2008**, *70*, 1919–1928.
7. Amores, A.; Monserrat, S.; Marcos, M.; Argüeso, D.; Villalonga, J.; Jordà, G.; Gomis, D. Numerical simulation of atmospheric lamb waves generated by the 2022 hunga-tonga volcanic eruption. *Geophys. Res. Lett.* **2022**, *49*, e2022GL098240. [[CrossRef](#)]
8. Lin, J.T.; Rajesh, P.K.; Lin, C.C.; Chou, M.Y.; Liu, J.Y.; Yue, J.; Hsiao, T.Y.; Tsai, H.F.; Chao, H.M.; Kung, M.M. Rapid conjugate appearance of the giant ionospheric lamb wave signatures in the northern hemisphere after hunga-tonga volcano eruptions. *Geophys. Res. Lett.* **2022**, *49*, e2022GL098222.
9. Barberi, F.; Bertagnini, A.; Landi, P.; Principe, C. A review on phreatic eruptions and their precursors. *J. Volcanol. Geotherm. Res.* **1992**, *52*, 231–246.
10. Del Negro, C.; Currenti, G.; Napoli, R.; Vicari, A. Volcanomagnetic changes accompanying the onset of the 2002–2003 eruption of mt. Etna (Italy). *Earth Planet. Sci. Lett.* **2004**, *229*, 1–14. [[CrossRef](#)]
11. Hurst, A.; Rickerby, P.; Scott, B.; Hashimoto, T. Magnetic field changes on white island, new zealand, and the value of magnetic changes for eruption forecasting. *J. Volcanol. Geotherm. Res.* **2004**, *136*, 53–70.
12. Adushkin, V.; Rybnov, Y.S.; Spivak, A. *Geophysical Effects of the Eruption of Hunga–Tonga–Hunga–Ha’apai Volcano on 15 January 2022*; Doklady Earth Sciences; Springer: Berlin/Heidelberg, Germany, 2022; pp. 362–367.
13. Ciraolo, L.; Spalla, P. Comparison of ionospheric total electron content from the navy navigation satellite system and the gps. *Radio Sci.* **1997**, *32*, 1071–1080. [[CrossRef](#)]
14. Arikan, F.; Erol, C.; Arikan, O. Regularized estimation of vertical total electron content from global positioning system data. *J. Geophys. Res. Space Phys.* **2003**, *108*, 1469. [[CrossRef](#)]
15. Nayir, H.; Arikan, F.; Arikan, O.; Erol, C. Total electron content estimation with reg-est. *J. Geophys. Res. Space Phys.* **2007**, *112*, A11313.
16. Feltens, J. Chapman profile approach for 3-d global tec representation. In Proceedings of the IGS AC Workshop, Dramstadt Germany, 9–11 February 1998; pp. 285–297.
17. Wen, D.; Mei, D. Ionospheric tec disturbances over China during the strong geomagnetic storm in September 2017. *Adv. Space Res.* **2020**, *65*, 2529–2539. [[CrossRef](#)]
18. Hoffmann, L.; Alexander, M.J. Occurrence frequency of convective gravity waves during the north american thunderstorm season. *J. Geophys. Res. Atmos.* **2010**, *115*, D20111.
19. Hoffmann, L.; Xue, X.; Alexander, M. A global view of stratospheric gravity wave hotspots located with atmospheric infrared sounder observations. *J. Geophys. Res. Atmos.* **2013**, *118*, 416–434.
20. Huang, T.Y.; George, R. Simulations of gravity wave-induced variations of the oh (8, 3), o2 (0, 1), and o (1s) airglow emissions in the mlt region. *J. Geophys. Res. Space Phys.* **2014**, *119*, 2149–2159.
21. Ern, M.; Hoffmann, L.; Rhode, S.; Preusse, P. The mesoscale gravity wave response to the 2022 tonga volcanic eruption: Airs and mls satellite observations and source backtracing. *Geophys. Res. Lett.* **2022**, *49*, e2022GL098626.
22. Mandal, S.; Pallamraju, D. Thermospheric gravity wave characteristics in the daytime over low-latitudes during geomagnetic quiet and disturbed conditions. *J. Atmos. Sol. -Terr. Phys.* **2020**, *211*, 105470.
23. Azeem, I.; Barlage, M. Atmosphere-ionosphere coupling from convectively generated gravity waves. *Adv. Space Res.* **2018**, *61*, 1931–1941. [[CrossRef](#)]
24. Schellart, W.; Lister, G.; Toy, V. A late cretaceous and cenozoic reconstruction of the southwest pacific region: Tectonics controlled by subduction and slab rollback processes. *Earth-Sci. Rev.* **2006**, *76*, 191–233. [[CrossRef](#)]
25. Brenna, M.; Cronin, S.J.; Smith, I.E.M. Post-caldera volcanism reveals shallow priming of an intra-ocean arc andesitic caldera: Hunga volcano, tonga, sw pacific. *Lithos: Int. J. Mineral. Petrol. Geochem.* **2022**, *412*, 106614. [[CrossRef](#)]
26. Long, T. Ionospheric disturbances of the 15 January 2022, tonga volcanic eruption observed using the gnss network in new zealand. *GPS Solut.* **2023**, *27*, 53.
27. Marchetti, D.; Zhu, K.; Zhang, H.; Zhima, Z.; Yan, R.; Shen, X.; Chen, W.; Cheng, Y.; He, X.; Wang, T. Clues of lithosphere, atmosphere and ionosphere variations possibly related to the preparation of La Palma 19 September 2021 volcano eruption. *Remote Sens.* **2022**, *14*, 5001. [[CrossRef](#)]

28. Yuen, D.A.; Scruggs, M.A.; Spera, F.J.; Zheng, Y.; Hu, H.; McNutt, S.R.; Thompson, G.; Mandli, K.; Keller, B.R.; Wei, S.S. Under the surface: Pressure-induced planetary-scale waves, volcanic lightning, and gaseous clouds caused by the submarine eruption of hunga tonga-hunga ha'apai volcano. *Earthq. Res. Adv.* **2022**, *2*, 100134. [[CrossRef](#)]
29. Telesca, L.; Lovallo, M.; Flores-Marquez, E.L. Characterizing volcanic states at popocatepetl, mexico by informational analysis of continuous geomagnetic signal. *Phys. A Stat. Mech. Its Appl.* **2017**, *487*, 178–184. [[CrossRef](#)]
30. Wallace, J.M.; Hobbs, P.V. *Atmospheric Science: An Introductory Survey*; Elsevier: Amsterdam, The Netherlands, 2006; Volume 92.
31. Pulinets, S.; Ouzounov, D. Lithosphere–atmosphere–ionosphere coupling (laic) model—An unified concept for earthquake precursors validation. *J. Asian Earth Sci.* **2011**, *41*, 371–382. [[CrossRef](#)]
32. Pulinets, S.A. Physical mechanism of the vertical electric field generation over active tectonic faults. *Adv. Space Res.* **2009**, *44*, 767–773. [[CrossRef](#)]
33. Kanamori, H.; Mori, J.; Harkrider, D.G. Excitation of atmospheric oscillations by volcanic eruptions. *J. Geophys. Res. Solid Earth* **1994**, *99*, 21947–21961. [[CrossRef](#)]
34. Kaladze, T.; Misra, A.; Roy, A.; Chatterjee, D. Nonlinear evolution of internal gravity waves in the earth's ionosphere: Analytical and numerical approach. *Adv. Space Res.* **2022**, *69*, 3374–3385. [[CrossRef](#)]
35. Liu, X.; Xu, J.; Yue, J.; Kogure, M. Strong gravity waves associated with tonga volcano eruption revealed by saber observations. *Geophys. Res. Lett.* **2022**, *49*, e2022GL098339. [[CrossRef](#)]

**Disclaimer/Publisher's Note:** The statements, opinions and data contained in all publications are solely those of the individual author(s) and contributor(s) and not of MDPI and/or the editor(s). MDPI and/or the editor(s) disclaim responsibility for any injury to people or property resulting from any ideas, methods, instructions or products referred to in the content.